Role of Atlantic multidecadal variability in modulating Arctic sea ice loss and wetting

ATMOSPHERIC SCIENCE

Role of Atlantic multidecadal variability in modulating Arctic sea ice loss and wetting

Ziyi Cai[1], Qinglong You[1]*, James A. Screen[2], Hans W. Chen[3], Ruonan Zhang[1], Zhiyan Zuo[1], Deliang Chen[4], Judah Cohen[5,6], Shichang Kang[7]*, Weiming Ma[8], Sergey K. Gulev[9], G. W. K. Moore[10,11], Renhe Zhang[1]

Arctic precipitation has increased in recent decades (hereafter, Arctic wetting), but the drivers remain uncertain. Using observations, reanalyses, and single-model initial-condition large ensembles (SMILEs), we show that enhanced evaporation due to sea ice loss has been the primary driver of Arctic wetting during 1979–2024, especially in the Atlantic sector. However, the externally forced component in most SMILEs explains only ~69% of sea ice loss and 75% of wetting in the observations and reanalyses. Further analysis reveals that the observed transition of one of the Northern Hemisphere's interdecadal internal variability—Atlantic multidecadal variability (AMV)—from a negative to a positive phase substantially enhanced Arctic sea ice loss, thereby accelerating wetting by about 31%. Under SSP3-7.0, if the AMV switches phase in the near future from the current +1 to a −1 standard deviation anomaly, then the rates of Arctic sea ice loss and wetting would slow by nearly 29 and 33%, respectively, relative to the externally forced response alone. These results underscore the pivotal role of AMV in modulating Arctic sea ice loss and wetting and highlight the need to account for AMV phase changes in near-term Arctic climate projections.

INTRODUCTION

Arctic precipitation is increasing (*1*), hereafter referred to as Arctic wetting (*2*), with a shift from snowfall to rainfall dominance (*3*). While these changes are evident throughout the circumpolar Arctic, substantial regional variations exist (*2*). Moreover, these changes are expected to intensify in the future, leading to severe environmental consequences (*4*). For instance, the accelerated water cycle may hasten the retreat of cryospheric elements such as sea ice (*5*–*7*), the Greenland Ice Sheet (*8*), and permafrost (*9*); increase freshwater input into the ocean, affecting ocean circulation; disrupt Arctic ecosystems; and pose threats to the Arctic social conditions (*10*, *11*). Despite increased intensity of Arctic atmospheric rivers (*12*), the mean poleward moisture transport to the Arctic has not shown a pronounced increase in recent decades, whereas both Arctic atmospheric moisture content and total precipitation have increased significantly during the same period (*13*, *14*). This raises questions about the underlying mechanisms. Many studies have suggested that enhanced evaporation due to sea ice loss and the expansion of open water areas is a dominant driver of Arctic precipitation changes, both historically and in future projections (*2*, *15*). However, the mechanisms underlying this linkage remain insufficiently understood. Identifying the drivers of Arctic sea ice loss and wetting and accurately projecting them are essential for developing effective environmental policies for the Arctic.

In addition, climate models exhibit large uncertainties in their projections of Arctic precipitation (*16*, *17*). Simulations driven by historical forcing underestimate mean Arctic precipitation and its trend compared to observations and reanalyses (*2*). These uncertainties arise partly from the inaccuracy of the representation of advective processes in climate models, parameterizations, and underlying assumptions (*18*, *19*). In addition, internal climate variability can critically modulate recent Arctic climate change (*20*–*22*), contributing 40 to 50% of the recently observed Arctic sea ice loss (*23*), especially in the Barents Sea (*24*). When the influence of internal variability is removed, the Arctic amplification ratio decreases from approximately four to three times the global mean warming rate (*25*). The two coupled ocean-atmosphere interdecadal modes in the Northern Hemisphere—the Atlantic multidecadal variability (AMV) and the interdecadal Pacific oscillation (IPO)—have far-reaching impacts in the Arctic (*26*–*28*). Phase transitions in the AMV and IPO contribute to regulating poleward oceanic and atmospheric energy transport, which affects Arctic warming (*29*), sea ice loss (*22*), and Arctic atmospheric rivers (*12*) on multidecadal timescales. For example, idealized pacemaker experiments isolating the climate impacts of AMV and IPO show that during the positive phase of AMV, atmospheric teleconnections can lead to an increased prevalence of the Arctic Dipole sea level pressure (SLP) pattern, driving sea ice loss through anomalous wind forcing and anomalous atmospheric energy transport (*30*–*32*); the positive phase of IPO triggers atmospheric teleconnections from the tropical Pacific through the Pacific to northern Canada, forming a quasi-barotropic structure at mid-to-high latitudes, promoting warming and sea ice loss in the Pacific–North American region (*26*, *33*). Accounting for the evolution of interdecadal internal variability is essential for reducing the uncertainty in near-term future climate projections (*34*, *35*), these modes of variability can either accelerate or dampen anthropogenic Arctic climate change in the

[1]Department of Atmospheric and Oceanic Sciences & Institute of Atmospheric Sciences & Key Laboratory of Polar Atmosphere-Ocean-Ice System for Weather and Climate, Ministry of Education, Fudan University, Shanghai 200438, China. [2]Department of Mathematics and Statistics, University of Exeter, Exeter, UK. [3]Chalmers University of Technology, Department of Space, Earth and Environment, SE-412 96 Gothenburg, Sweden. [4]Department of Earth System Sciences, Tsinghua University, Beijing 100084, China. [5]Atmospheric and Environmental Research Inc., Lexington, MA, USA. [6]Department of Civil and Environmental Engineering, Massachusetts Institute of Technology, Cambridge, MA, USA. [7]Key Laboratory of Cryospheric Sciences and Frozen Soil Engineering, Northwest Institute of Eco-Environment and Resources, Chinese Academy of Sciences, Lanzhou 730000, China. [8]Atmospheric, Climate, and Earth Sciences Division, Pacific Northwest National Laboratory, Richland, WA, USA. [9]P.P. Shirshov Institute of Oceanology, Russian Academy of Sciences, Moscow, Russia. [10]Department of Chemical and Physical Sciences, University of Toronto Mississauga, Mississauga, ON, Canada. [11]Department of Physics, University of Toronto, Toronto, ON, Canada.
*Corresponding author. Email: qlyou@fudan.edu.cn (Q.Y.); shichang.kang@lzb.ac.cn (S.K.)

coming decades (*36*). However, the mechanisms through which internal variability influences Arctic wetting, along with the corresponding quantitative estimates, remain poorly understood. This study uses single-model initial-condition large ensembles (SMILEs) to investigate how interdecadal internal variability has influenced Arctic wetting and its underlying mechanisms over the recent decades. It also quantifies how Arctic wetting could be influenced by phase shifts in the AMV in the near-term future, providing mechanistic insights that can contribute to future constraints on Arctic climate projection uncertainties.

RESULTS

Local sea ice loss contributes to historical Arctic wetting

Multiple reanalysis datasets indicate an increased Arctic total precipitation from 1979 to 2024 at an average rate of 0.03 mm/day per decade, with consistency across datasets (Fig. 1A). We examined the spatial patterns of Arctic precipitation trends as depicted by European Centre for Medium-Range Weather Forecasts (ECMWF) Reanalysis v5 (ERA5) and Japanese 55-year Reanalysis (JRA55) (Fig. 1B and fig. S1), since these two datasets outperform other reanalysis datasets in capturing Arctic precipitation trend, with better agreement when compared to observational site data (*2*). The results show that increased precipitation is primarily concentrated in the eastern Arctic, particularly in the Barents-Kara seas (BKS; 70°N to 80°N, 30°E to 90°E). In contrast, the western Arctic, especially the North American Arctic, shows negligible changes. This pattern aligns with observations from Global Historical Climatology Network monthly data (*2*). The results of moisture budget analysis (see Materials and Methods) reveal that the observed annual mean precipitation increase from 1979 to 2024 is primarily driven by enhanced evaporation, contributing a growth of 0.02 mm/day per decade, especially in the BKS region (Fig. 1C and fig. S1). The time series of horizontal atmospheric

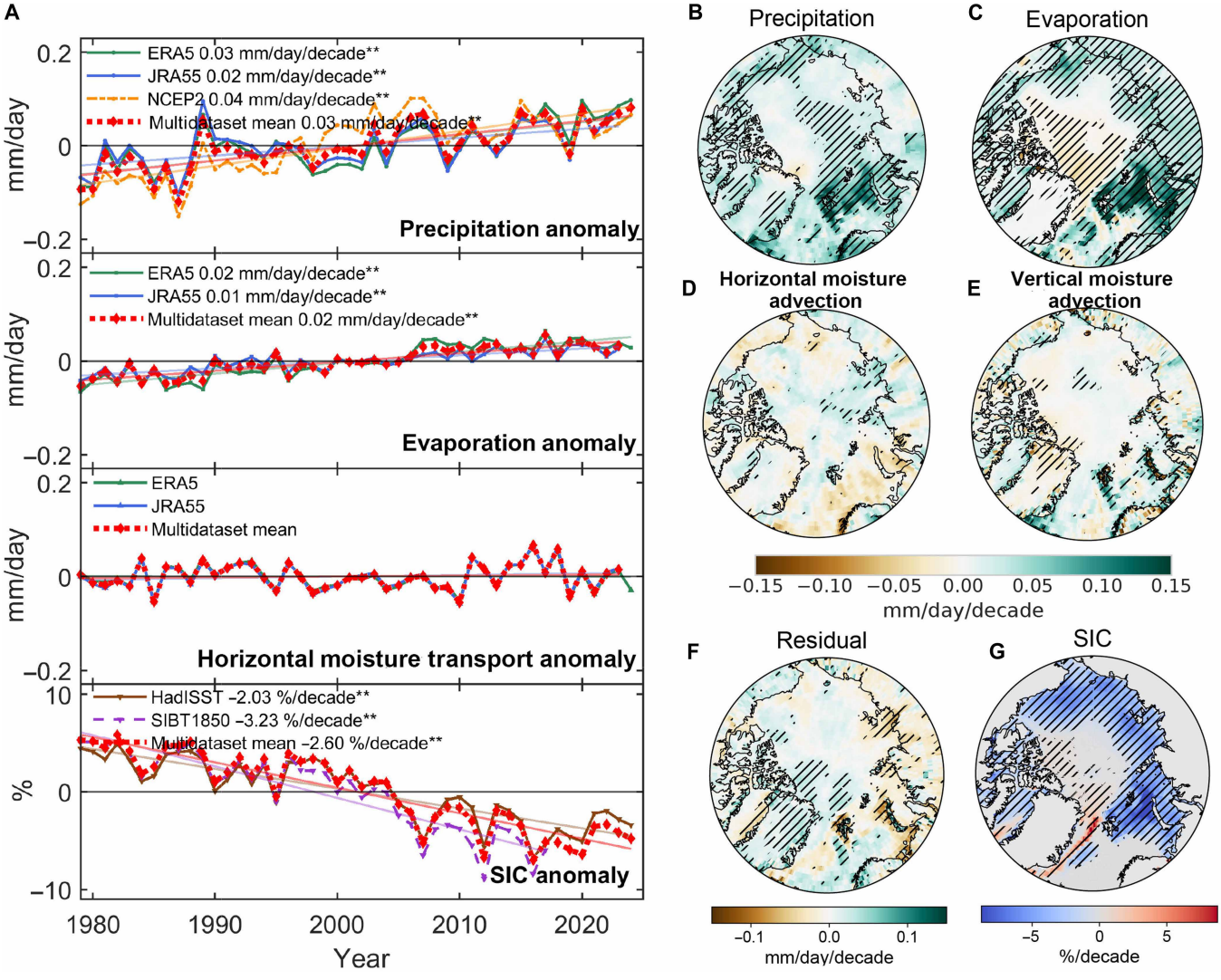

Fig. 1. Observed Arctic wetting and sea ice concentration changes from 1979 to 2024. (**A**) Time series of anomalies of moisture budget terms and sea ice concentration (SIC) from different datasets. Spatial pattern of trends in moisture budget terms trends from ERA5, including (**B**) Arctic total precipitation, (**C**) evaporation, (**D**) horizontal moisture advection, (**E**) vertical moisture advection term, and (**F**) residual term. (**G**) Spatial pattern of Arctic sea ice trend from the Hadley Center. Double asterisks (**) in (A) and hatched areas in [(B) to (G)] indicate where linear trends are statistically significant at the 95% confidence level.

moisture transport exhibits pronounced interannual variability but shows no significant trend contribution over the entire period, which is also reflected in the spatial patterns (Fig. 1D). The contribution of the vertical moisture transport trend is also weak (Fig. 1E), while the residual terms show significant increases over eastern Greenland (Fig. 1F), where pronounced topographical relief may induce surface processes. The spatial pattern of sea ice loss is consistent with that of enhanced evaporation and precipitation (Fig. 1G), suggesting a signal coupling between them. Sea ice loss expands open water, which strengthens local evaporation and primarily drives the increase in precipitation, while the resulting wetter and warmer atmosphere further promotes sea ice loss.

To separate the roles of external forcing and internal variability in the observed Arctic sea ice loss and wetting, we used eight SMILEs (see Materials and Methods). Since different ensemble members within each SMILE are driven by the same external forcing, their ensemble mean can represent the effects of external forcing such as CO_2 increase, while the spread between members reflects the influence of internal variability (*37*). The ensemble mean of most SMILEs explains only 69% (46 to 98%), 59% (43 to 91%), and 75% (59 to 102%) of the Arctic sea ice loss (Fig. 2, A to C) and increased evaporation and precipitation from reanalyses during the historical period, respectively, except for CanESM5, which has been identified in previous studies as having high equilibrium climate sensitivity and reflecting excessive global warming (*38*). When focusing on the eastern Arctic region where wetting is most pronounced, the ensemble means of SMILEs significantly underestimate the enhancement of Arctic sea ice loss, evaporation, and precipitation, especially over the BKS region, by 37% (14 to 57%), 42% (20 to 75%), and 33% (12 to 42%), respectively (Fig. 2, D to F). Notably, these discrepancies may be partly influenced by biases in the reanalyses themselves, as one previous study has reported that reanalysis data such as ERA5 may overestimate Arctic mean temperature and precipitation (*39*). Meanwhile, the intermember spread of simulated sea ice loss and wetting in this region is also the largest among SMILEs (Fig. 2, G to I). This indicates that internal variability plays an important role in recent Arctic coupled sea ice loss and wetting.

The important role of AMV in Arctic sea ice loss and wetting

To investigate whether the Arctic wetting is influenced by large-scale modes of sea surface temperature (SST) variability, we first applied the maximum covariance analysis (MCA) to the internally generated Arctic precipitation trends and global SST trends during 1979–2024 across all 50 ensemble members of Community Earth System Model version 2 (CESM2). The first mode explains ~55% of the covariance, showing intensified precipitation across most Arctic regions, especially in the Atlantic sector in the eastern Arctic (Fig. 3A), with an SST pattern resembling a positive AMV phase in the North Atlantic and warming in the North Pacific (Fig. 3B). The second mode explains 10% of the variance and exhibits a dipole pattern, with enhanced precipitation in the east and decreased precipitation in the west (Fig. 3C), corresponding to a positive AMV phase in the North Atlantic and a negative IPO phase in the Pacific (Fig. 3D). We also examined the MCA analysis results of other SMILEs that can reasonably simulate AMV or IPO (see Materials and Methods) to verify whether this synergistic pattern is model dependent. The results found that the Arctic wetting and positive AMV phase shown in the first mode are quite consistent across models (figs. S2 and S3). Meanwhile, the AMV trend during the study period is significantly positively correlated with Arctic wetting in all models, with correlation coefficients exceeding 0.5 in most SMILEs (Fig. 3E), which suggests that the Arctic wetting is modulated by the AMV.

On the basis of results from multiple observational and reanalysis datasets, when the influence of IPO is filtered out through regression, increases in the AMV index are strongly associated with an intensification of sea ice loss in the Atlantic sector of the Arctic, which subsequently drives enhanced evaporation accompanied by increased precipitation, with the most pronounced changes in the BKS region (fig. S4). All SMILEs exhibit a similar Arctic wetting and sea ice loss pattern associated with AMV change (figs. S5 to S7). However, the linkage between IPO and Arctic wetting is relatively weak (Fig. 3E). This may be because the influence of the IPO on the Arctic relies on complex tropical–high latitude atmospheric teleconnection pathways (*40*, *41*), while model biases in simulating IPO-related SST patterns lead to discrepancies in the associated Rossby wave trains (*42*). In addition, other atmospheric internal variability also plays an important role in modulating the Pacific-Arctic climate linkage, and the relative interactions between the IPO and other modes across different timescales remain unclear (*23*, *43*). In summary, the above results indicate that AMV is the primary coupled ocean-atmosphere interdecadal mode regulating recent Arctic coupled sea ice loss and wetting and that this linkage is consistent across SMILEs. After applying observational AMV adjustments in SMILEs (see Materials and Methods), the explained Arctic sea ice loss and wetting during the historical period are substantially increased (fig. S8), with AMV accelerating Arctic sea ice loss and its corresponding enhanced evaporation and precipitation by 33% (28 to 37%), 38% (33 to 44%), and 31% (25 to 43%), respectively, on top of external forcing.

Mechanisms of the AMV phase changes in driving Arctic sea ice loss and wetting

By analyzing the differences among ensemble members within the same SMILE, the mechanisms by which AMV changes affect internally generated Arctic wetting can be determined. Here, we used the CESM2 model, which simulates the AMV and its associated Arctic sea ice loss and wetting pattern well and has large ensemble members for future projections. Five ensemble members from the CESM2 with the largest AMV trend from 1979 to 2024 (AMV+5) and the five with the smallest AMV trend (AMV−5) were selected. AMV+5 exhibited a phase transition from negative to positive, consistent with observations, while AMV−5 showed the opposite trend (Fig. 4A). Composite analysis (AMV+5 minus AMV−5) reveals significant sea ice loss, enhanced evaporation, and increased precipitation in the Arctic Atlantic sector (Fig. 4, B to D). The members were divided into three groups based on the AMV phase changes (Fig. 4, E to G): those with significant positive phase transitions, significant negative phase transitions, and no significant transitions (see Materials and Methods). Ensemble members with significant positive AMV changes showed stronger actual SST warming closer to observations, while those with negative changes exhibited weaker actual SST warming (fig. S9). Correlation analysis between the members indicated that significant AMV phase changes correspond to larger trends in Arctic sea ice concentration (SIC), evaporation, and precipitation. Crucially, when AMV changes were insignificant, precipitation showed no significant trend. When sea ice remained nearly unchanged (Fig. 4F), AMV phase changes had minimal impact on evaporation and precipitation (Fig. 4, G to F). This suggests that AMV phase changes influence Arctic wetting through local sea ice loss.

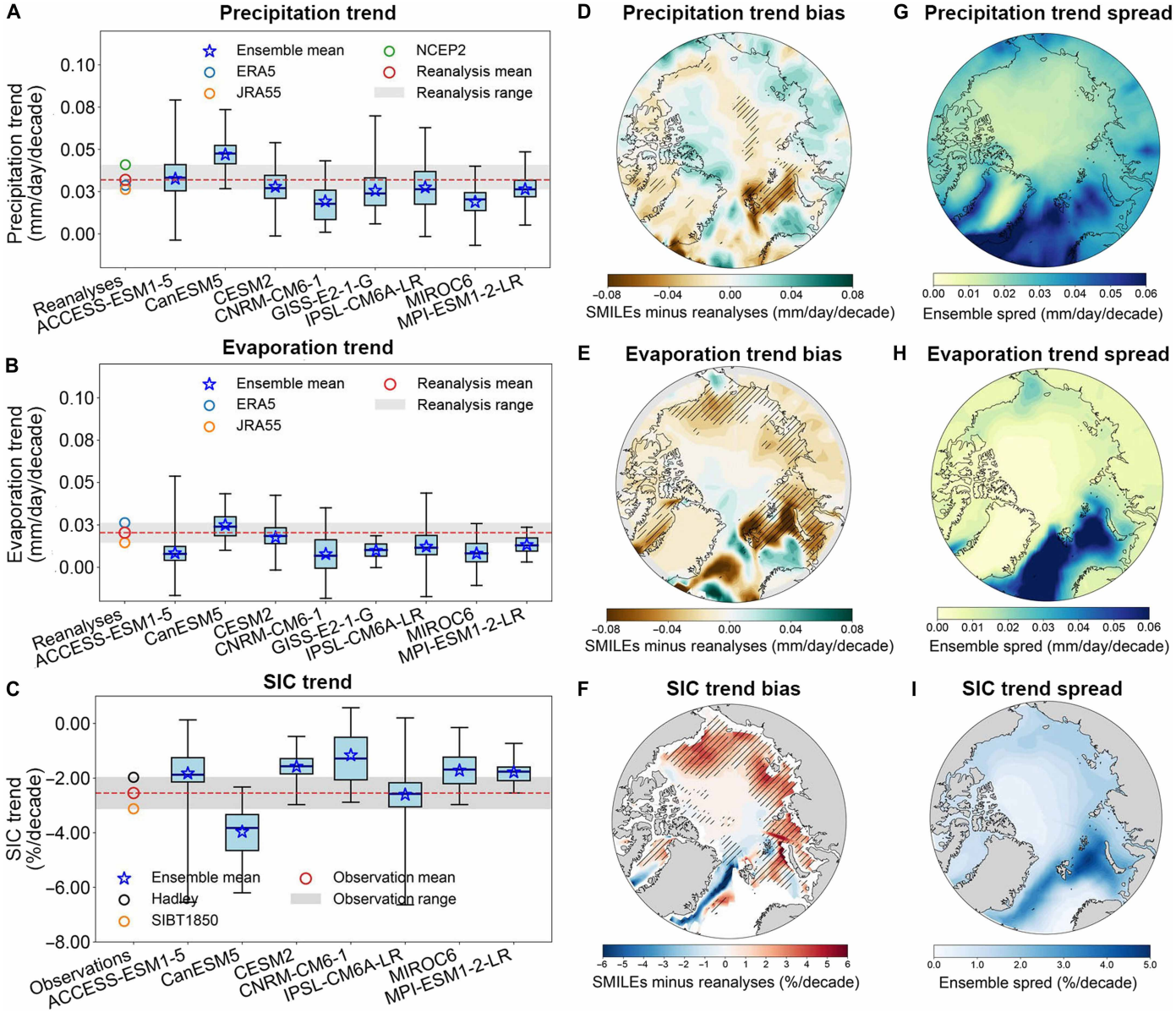

Fig. 2. Simulated Arctic wetting and SIC changes in the historical period. Arctic-mean trends in (**A**) precipitation, (**B**) evaporation, and (**C**) SIC from large-ensemble model simulations and multiple reanalysis datasets. The red dashed line denotes the mean across the observations/reanalyses; gray shading indicates their range; boxes show the interquartile range (25th to 75th percentiles) for each model; whiskers indicate the full range (minimum to maximum); and stars mark the ensemble mean. (**D**) Spatial pattern of differences between Arctic precipitation trends simulated by eight large-ensemble models and those from the reanalyses (multimodel ensemble mean minus the reanalyses mean); hatched areas indicate where linear trends are significant at the 95% confidence level in both the models and the observations/reanalyses. (**E**) The same as (D) but for evaporation. (**F**) The same as (D) but for SIC. (**G**) Multimodel mean spatial pattern of the interensemble spread in precipitation trends. (**H**) The same as (G) but for evaporation. (**I**) The same as (G) but for SIC. To ensure consistent data coverage across observations/reanalyses and all models, the analysis period spans 1979–2014.

We further examined the impacts of AMV on internally generated ocean heat transport (OHT). Previous studies have shown that AMV changes are associated with the Atlantic Meridional Overturning Circulation (AMOC), where enhanced AMOC favors positive AMV formation and strengthens OHT to the Arctic (*44*, *45*). AMV+5 displays significantly enhanced OHT (from the surface to subsurface) through the Barents Sea Opening (BSO) from the Atlantic sector to the eastern Arctic basin (Fig. 5A), compared to AMV−5, accompanied by significant warming in the 0- to 300-m layer of the Arctic Atlantic sector (Fig. 5B). We calculated the zonally integrated OHT anomaly through the BSO as OHT BSO (see Materials and Methods) and examined its relationship with AMV changes and related oceanic conditions in the Arctic across ensemble members. It is shown that AMV phase changes are significantly positively correlated with OHT BSO changes ($r = 0.59$, $P < 0.05$; Fig. 5C), OHT BSO is positively correlated with the upper 300-m layer ocean temperature trends in the Atlantic sector ($r = 0.69$, $P < 0.05$; Fig. 5D), which, in turn, correlate negatively with SIC trends ($r = -0.82$,

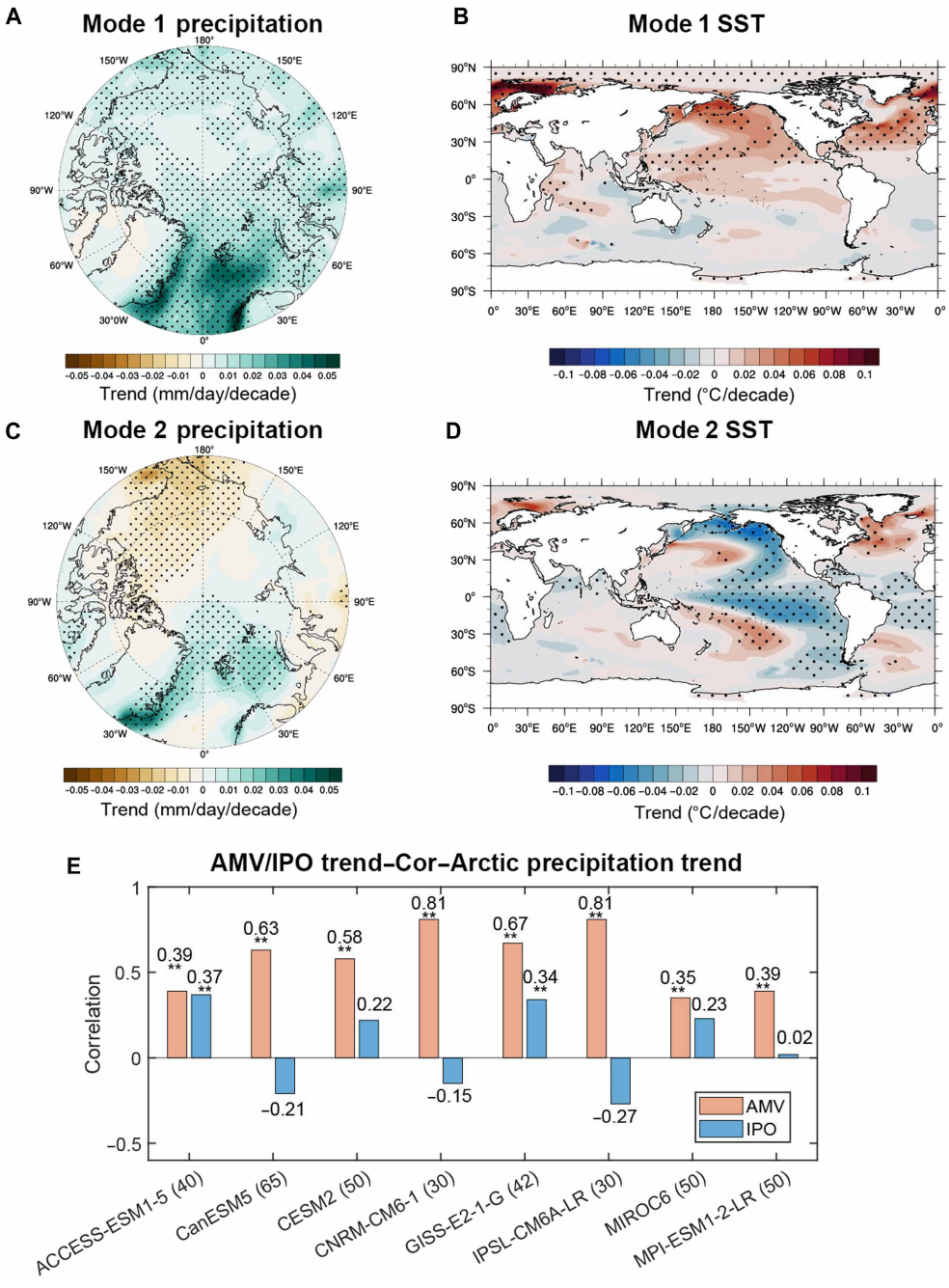

Fig. 3. The covariability between the Arctic wetting trend and the global SST trend driven by internal variability. Spatial pattern of the Arctic wetting trend associated with the (**A**) first and (**C**) second mode of MCA. (**B** and **D**) The same as (A) and (C) but for the global SST trend. The ensemble mean trends of both the Arctic wetting and SST in the CESM2 have been removed from individual members before applying the MCA. The fraction of covariance explained by the first and second mode is 55 and 10%, respectively. These patterns are obtained by regressing the internally generated trends across 50 members from CESM2 onto their respective standardized expansion coefficients. Dotted areas indicate that regressions are significant at the 95% confidence level based on the Student's *t* test. (**E**) The correlation coefficients between AMV/IPO trends and Arctic average precipitation trends in models. Double asterisks (**) indicates that the correlation is significant at the 0.05 level.

$P < 0.05$; Fig. 5E). Therefore, during AMV transitions from negative to positive phase, enhanced OHT BSO promotes ocean warming in the Arctic Atlantic sector, further leading to sea ice loss. Meanwhile, those ensemble members with significant AMV transitions from negative to positive also better reproduced the observed interdecadal enhancement of BSO OHT during 1979–2024 (fig. S10). Thus, these results indicate that AMV influences sea ice loss by modulating OHT through the BSO, thereby contributing to local wetting.

AMV phase changes also alter internally generated atmospheric circulation. Compared to AMV−5, AMV+5 exhibits anomalous weakening of SLP over Greenland and its southern regions, while showing anomalous strengthening of SLP and 500-hPa geopotential

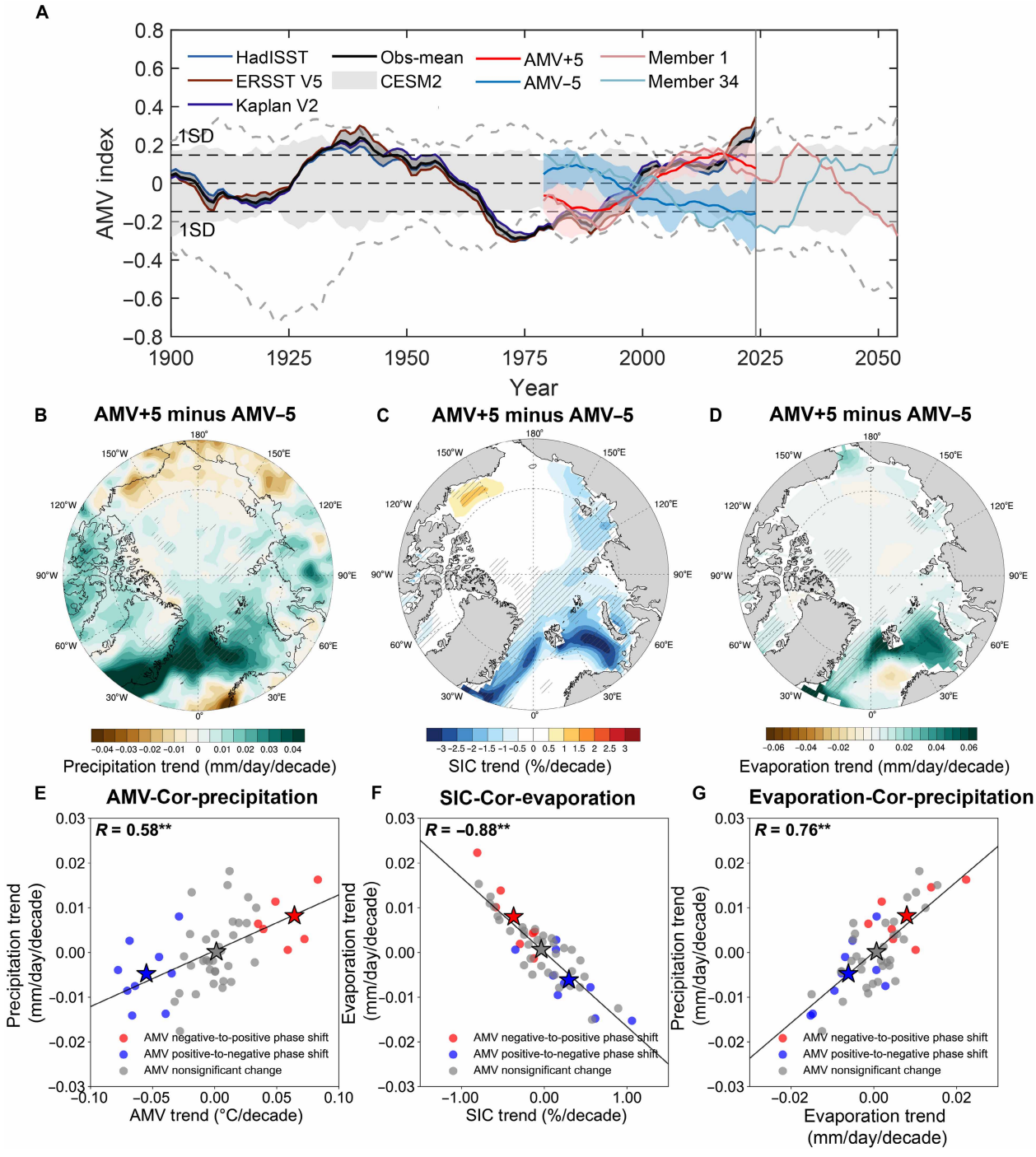

Fig. 4. The relationship between AMV changes and Arctic sea ice wetting coupling in CESM2. (**A**) Interdecadal changes of the observed and simulated AMV. Historical and SSP3-7.0 simulations are shown for the 5th and 95th percentiles (shading) and the maximum and minimum (dashed lines) of the 50 members. The black line represents the average of the three observational datasets [Hadley Centre sea ice and sea surface temperature (HadISST), Extended Reconstructed Sea Surface Temperature Version 5 (ERSST V5), and Kaplan Extended SST Version 2 (Kaplan V2)], and the dark-gray shading indicates the observational range (minimum to maximum). The results have been smoothed using an 11-year moving average. Member 1 represents an ensemble member where AMV transitions from −1 to 1 SD over the past four decades and from 1 to −1 SD in the near-term future, while member 34 is the opposite, representing two contrasting future AMV trajectories. (**B**) The total precipitation trend difference between the five members with the largest positive AMV phase changes and the five members with the largest negative AMV phase changes from 1979 to 2024. Hatched areas are statistically significant at the 90% confidence level according to the Student's *t* test. (**C** and **D**) The same as (B) but for SIC and evaporation trends. (**E**) The relationship between the AMV trend and the Arctic mean precipitation trend from 1979 to 2024 across 50 ensemble members. (**F**) The same as (E) but for the SIC trend and the Arctic mean evaporation trend. (**G**) The same as (E) but for the Arctic mean evaporation trend and the Arctic mean precipitation trend. Double asterisks (**) indicates a significant Pearson correlation ($P < 0.05$). Red (blue) dots indicate ensemble members in which the AMV transitions from a negative to a positive phase (from a positive to a negative phase) during 1979–2024, with the AMV index trend significant at the 95% confidence level according to the Student's *t* test. Gray dots indicate ensemble members with no significant AMV phase change.

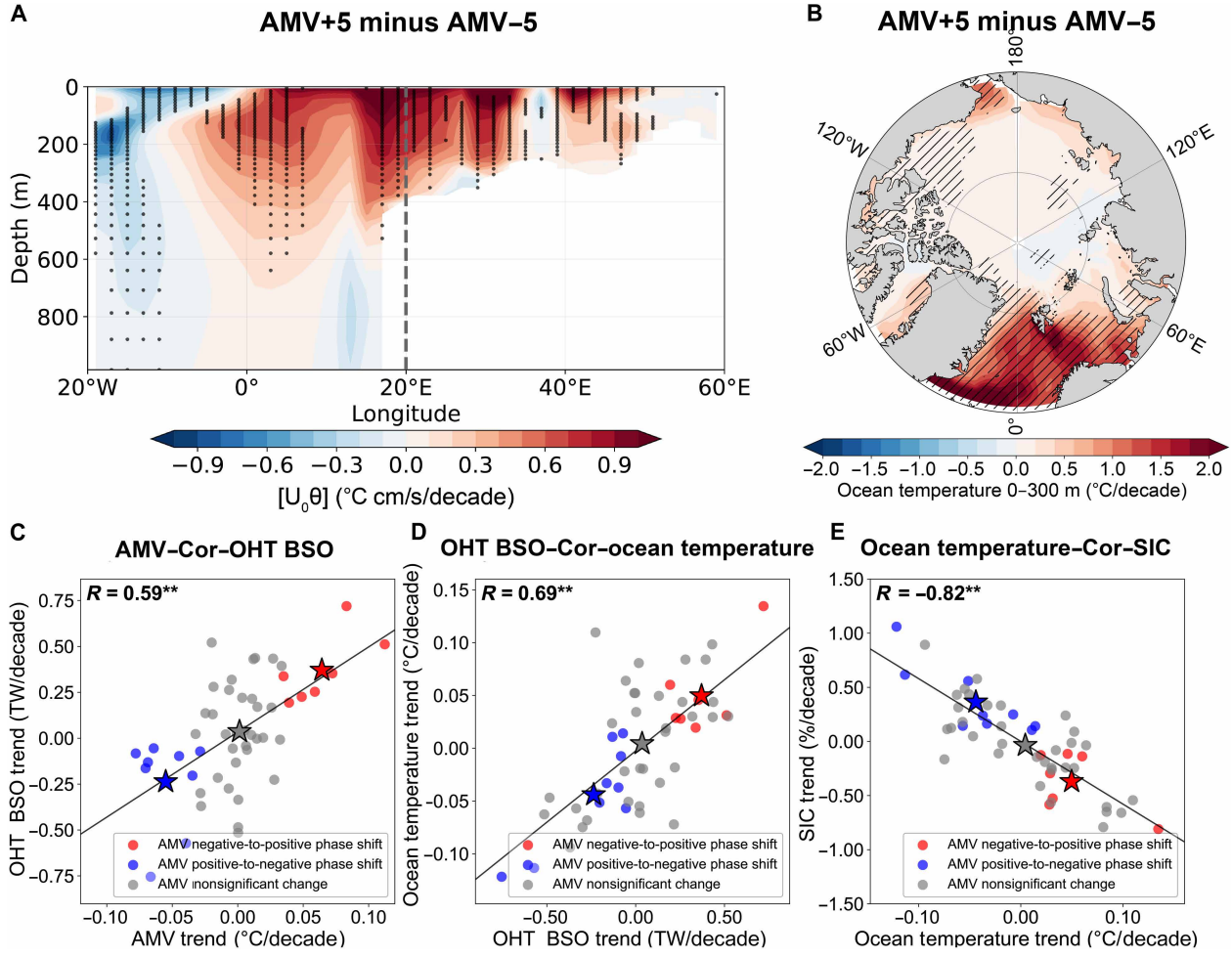

Fig. 5. The relationship between AMV changes and OHT over the North Atlantic in CESM2. (**A**) Longitude-depth profile of the difference in zonal oceanic heat transport $[U_0\theta]$ trend between the five members with the largest positive AMV phase changes and the five members with the largest negative AMV phase changes from 1979 to 2024. Dotted and hatched areas are statistically significant at the 90% confidence level according to the Student's *t* test. (**B**) The same as (A) but for the Arctic 0- to 300-m mean ocean temperature. (**C**) The relationship between the AMV trend and the OHT (through BSO, OHT BSO) trend from 1979 to 2024 across 50 ensemble members. (**D**) The same as (C) but for the OHT BSO trend and 0- to 300-m mean ocean temperature trend. (**E**) The same as (C) but for 0- to 300-m mean ocean temperature trend and Arctic SIC trend. Double asterisks (**) indicates a significant Pearson correlation ($P < 0.05$). Red (blue) dots indicate ensemble members in which the AMV transitions from a negative to a positive phase (from a positive to a negative phase) during 1979–2024, with the AMV index trend significant at the 95% confidence level according to the Student's *t* test. Gray dots indicate ensemble members with no significant AMV phase change.

height (Z500) over northern Eurasia to the BKS (Fig. 6A). This results in increased anomalous ascending motion over the Atlantic subpolar region (Fig. 6B) and descending motion over the BKS (Fig. 6C), with strengthened southerly winds from the Greenland Sea toward the Arctic (Fig. 6A). The transported moisture may enhance wetting over Greenland due to topographical uplifting (Fig. 4B). The strengthened Z500 and descending motion over the BKS increased atmospheric temperature, which promotes sea ice loss through enhanced downward longwave radiation, while sea ice loss can also intensify downward longwave radiation through atmospheric moistening, establishing a positive feedback that manifests as strong ice-atmosphere coupling in the BKS region. There is a positive correlation between AMV changes and BKS Z500 trends ($r = 0.49$, $P < 0.05$), a significant positive correlation between Z500 and downward longwave radiation trends ($r = 0.93$, $P < 0.05$), and a corresponding significant negative correlation with SIC trends ($r = -0.85$, $P < 0.05$) (Fig. 6, D to F). Similar AMV-related atmospheric circulation patterns are also found in reanalyses, although compared to CESM2, the positive SLP and Z500 anomalies in the reanalyses cover a broader area, with equally significant increased Z500 and descending motion over BKS (fig. S11). This may be related to the previously proposed mechanism whereby positive AMV phases cause northward migration of the Atlantic Intertropical Convergence Zone (*46*), generating upper-level divergence and Rossby wave trains at mid-high latitudes (*47*), leading to high-pressure anomalies from Eurasia to the Arctic (*26*). Meanwhile, the transition of AMV to its positive phase can intensify transient eddy activity by enhancing oceanic fronts and low-level atmospheric baroclinicity and subsequently drive negative North Atlantic oscillation/Arctic oscillation anomalies through wave-mean flow interactions (*12*, *48*), promoting increased geopotential height anomalies in the Arctic. Furthermore, sea ice loss reinforces the high-pressure anomaly through tropospheric warming and thermal

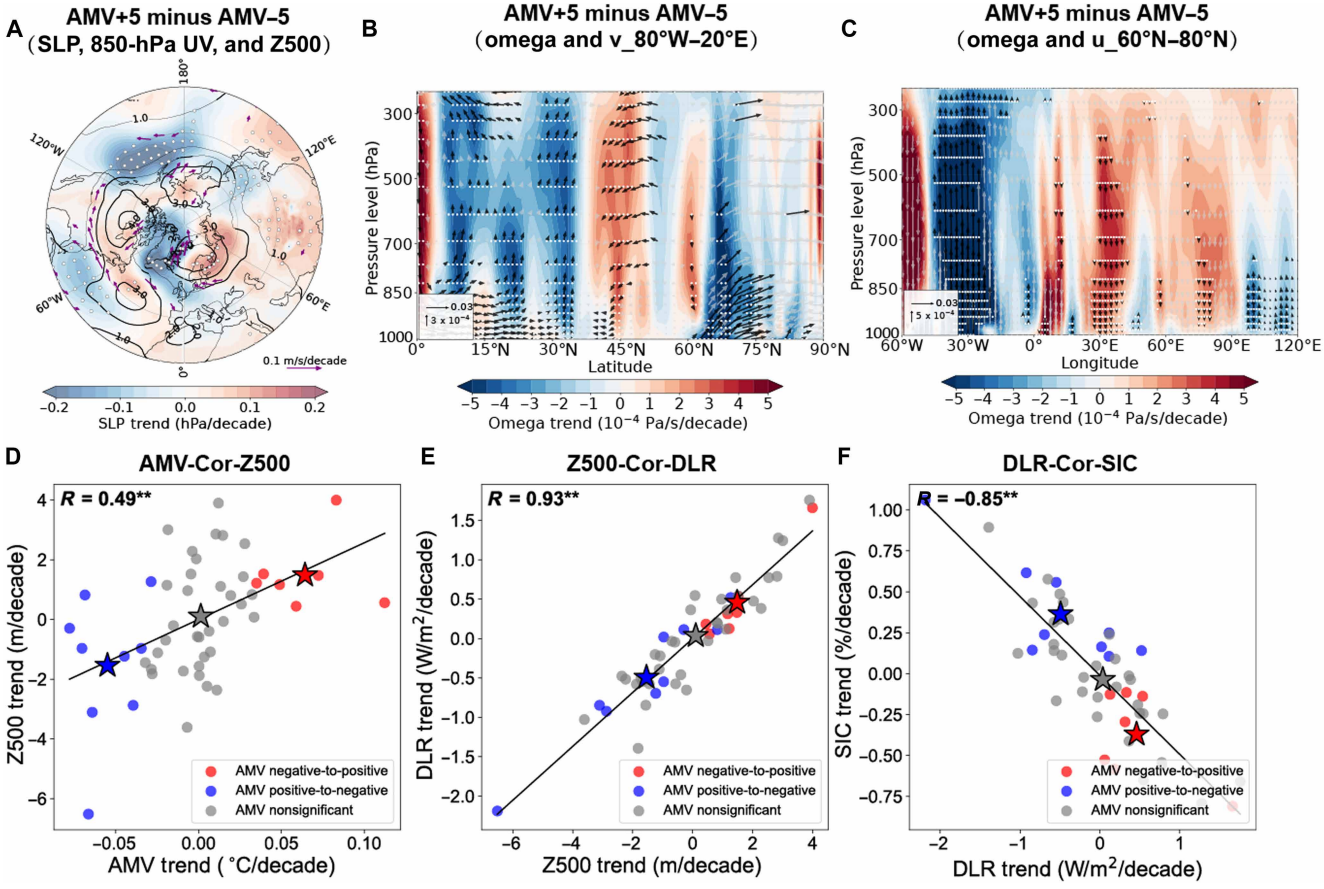

Fig. 6. The relationship between AMV changes and atmospheric circulation over the North Atlantic in CESM2. (**A**) The difference in SLP (shading), Z500 (contours), and horizontal wind (arrows) trends between the five members with the largest positive AMV phase changes and the five members with the largest negative AMV phase changes from 1979 to 2024. (**B**) The same as (A) but for the vertical circulation (vectors) and vertical velocity (shading) trends averaged along 80°W to 20°E. (**C**) The same as (A) but for the vertical circulation (vectors) and vertical velocity (shading) trends averaged along 60°N to 80°N. The results indicated by the bold contours, dotted areas, and arrows are shown to be statistically significant at the 90% confidence level according to the Student's *t* test. (**D**) The relationship between the AMV trend and Z500 trends over the BKS region from 1979 to 2024 across 50 ensemble members. (**E**) The same as (D) but for the Z500 trend and the clear-sky downward longwave radiation (DLR) trend. (**F**) The same as (D) but for the downward longwave radiation trend and the SIC trend. Double asterisks (**) indicates a significant Pearson correlation ($P < 0.05$). Red (blue) dots indicate ensemble members in which the AMV transitions from a negative to a positive phase (from a positive to a negative phase) during 1979–2024, with the AMV index trend significant at the 95% confidence level according to the Student's *t* test. Gray dots indicate ensemble members with no significant AMV phase change. Cor, correlation.

expansion, strengthening the ice-atmosphere coupling over the BKS region (*49*). To summarize, these findings support that AMV phase changes influence key regional sea ice loss and subsequent wetting through modifying OHT and modulating the atmospheric circulation.

Projections of near-term future Arctic sea ice loss and wetting constrained by AMV phase changes

Of the SMILEs that can well characterize the linkage between AMV and Arctic sea ice loss and wetting, CESM2 and MPI-ESM1-2-LR provide 50 ensemble members under the future SSP3-7.0 scenario and future SSP1-2.6/SSP2-4.5/SSP5-8.5 scenarios, respectively. Therefore, we used these two models to examine the impact of AMV on near-term future Arctic wetting. It is shown that Arctic wetting is expected to intensify in the near future (2025–2054). However, internal variability across the 50 ensemble members yields trends ranging from −0.02 to −0.04, −0.01 to −0.06, 0.00 to 0.06, and 0.01 to 0.07 mm/day per decade under the SSP1-2.6, SSP2-4.5, SSP3-7.0, and SSP5-8.5 scenarios, respectively. After excluding the influence of AMV (see Materials and Methods), the spread of trends across all ensemble members, as quantified by the SD, decreased by 11.6 to 20.2% under the four scenarios (fig. S12). These findings highlight that using initializing projections of AMV phase changes will increase confidence in near-term future Arctic wetting projections.

The impacts of AMV evolution on near-term future Arctic SIC, evaporation, and precipitation are quantified (Fig. 7). Given that the estimated SD of AMV from 1900 to 2014 is 0.15 and that the observed AMV has remained in a positive phase for over 20 years, we consider an illustrative and plausible scenario in which AMV will transition from +1 to −1 SD between 2025 and 2054, as illustrated by ensemble member 1 (Fig. 4A). This means that the AMV trends in the near-term future are fixed at −0.10°C per decade, which is similar to the magnitude of AMV change during historical periods. Next, we replaced the sea ice and wetting components associated with AMV changes in each member with the hypothetical AMV evolution. (see Materials and

Methods). Taking the SSP3-7.0 scenario as an example, for the transition from +1 to −1 SD of AMV, simulated sea ice loss will slow by 29% (from −3.17 to −2.26% per decade) on top of externally forced changes (Fig. 7A). At the same time, simulated intensification of evaporation will be mitigated (Fig. 7B), leading to Arctic wetting trends declining from 0.03 to 0.02 mm/day per decade (Fig. 7C). In contrast, when AMV transitions from −1 to +1 SD (as shown by ensemble member 34 in Fig. 4A), simulated sea ice loss will accelerate by 25%, leading to enhanced evaporation, which, in turn, increases wetting. Although this situation is unlikely to happen (since AMV is currently in a positive phase), the result indicates that AMV phase changes can continue to influence Arctic sea ice loss and wetting over the next 30 years. A more

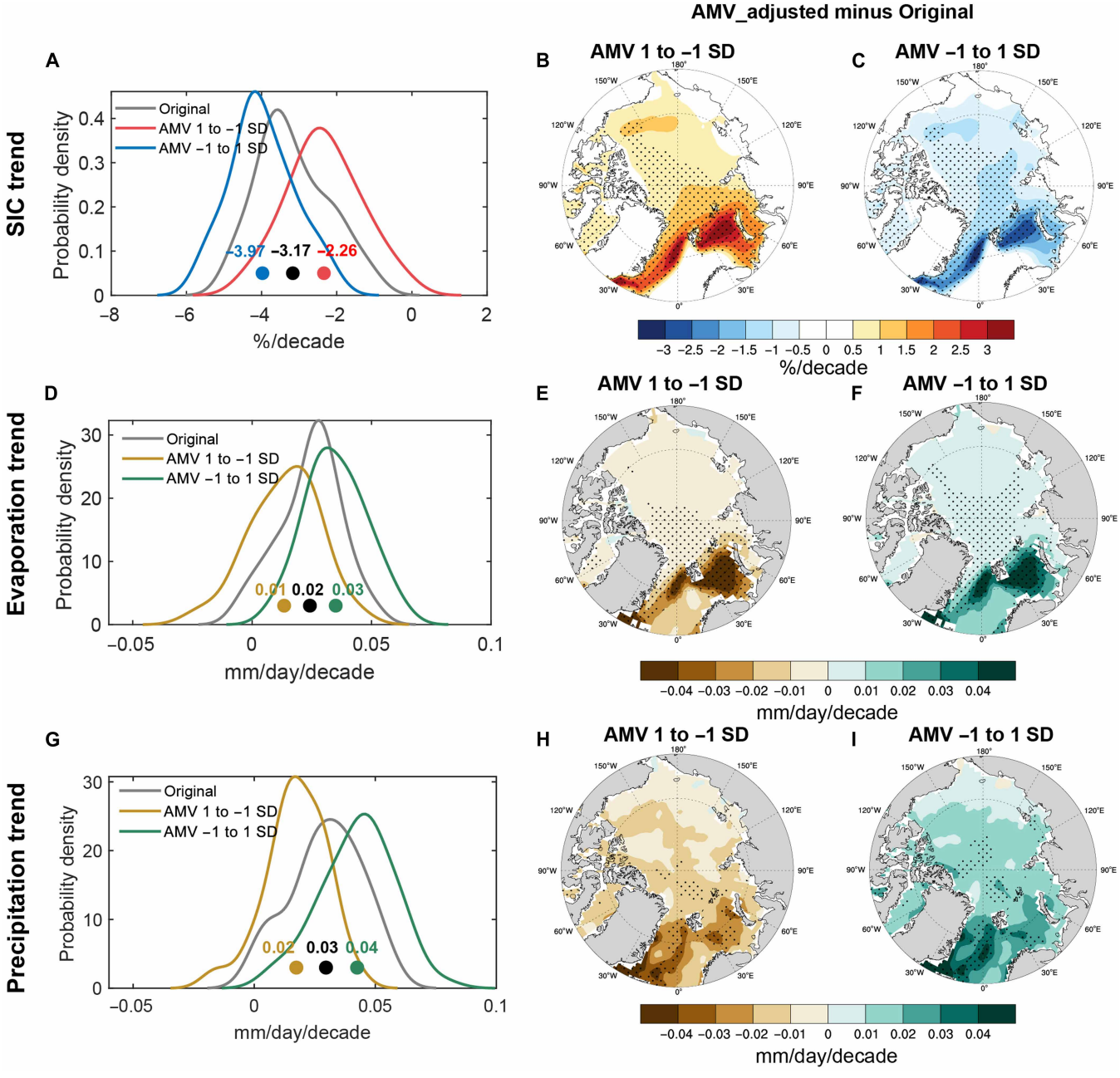

Fig. 7. The impact of AMV phase changes in the near-term Arctic SIC and wetting trends. (**A**) Histograms showing the frequency distribution of Arctic SIC trends in the near-term for the 50 members of CESM2, derived from the original results (gray line) and those adjusted to account for the influence of different AMV phase transitions (blue for −1 to +1 SD and red for +1 to −1 SD). The black dots represent the SIC trends for the ensemble mean without AMV adjustments, while the blue and red dots show the SIC trends for the ensemble mean with the respective AMV adjustments (blue for −1 to +1 SD and red for +1 to −1 SD). (**B**) The same as (A) but for evaporation. (**C**) The same as (A) but for total precipitation. (**D** and **E**) Spatial distribution difference of SIC trends before and after AMV adjustments (left: AMV transition from +1 to −1 SD; right: AMV transition from −1 to +1 SD) (adjusted trends minus original trends). (**F** and **G**) The same as (D) and (E) but for evaporation. (**H** and **I**) The same as (D) and (E) but for precipitation. Dotted areas are statistically significant at the 95% confidence level according to the Student's *t* test.

likely situation is that if AMV undergoes a 2-SD negative transition in the next 30 years, following historical cycles, it could dampen about 33% of the externally forced intensification of Arctic precipitation under the SSP3-7.0 scenario by mitigating Arctic sea ice loss. Similar results are found under the other three scenarios, where wetting could almost disappear under the SSP1-2.6 scenario, while under the SSP2-4.5 and SSP5-8.5 scenarios, it would suppress 36 and 26% of Arctic wetting, respectively (fig. S13). The spatial patterns obtained from similar adjustments at the grid level reveal that the impact of AMV phase changes on future Arctic wetting is most pronounced in the Greenland-Barents-Kara seas. Similar to historical periods, AMV phase changes have the most pronounced impact on sea ice and evaporation changes in this region (Fig. 7, D to I).

DISCUSSION

In summary, Arctic wetting has intensified over the past four decades, especially in the BKSs, primarily driven by increased evaporation linked to sea ice loss. In addition to external forcing, the coupled sea ice loss and wetting in the Arctic are also partially regulated by AMV. The transition of AMV from a negative to a positive phase strengthens OHT through the BSO. The accompanying atmospheric circulation anomalies feature positive geopotential height over the Arctic and enhanced descending motion over the BKS region, which increases downwelling longwave radiation, further amplifying the Arctic coupled sea ice loss and wetting, accelerating Arctic wetting by 31% (25 to 43%). The results further underscore the important role of AMV phase changes in shaping near-term future Arctic wetting. AMV explains 12 to 20% of the uncertainty in near-term Arctic wetting projections due to internal variability under different emissions scenarios. Taking the SSP3-7.0 scenario as an example, if the AMV phase shifts from +1 to −1 SD over the next 30 years, it could slow down the rate of Arctic sea ice loss and offset 33% of externally forced Arctic wetting.

Although many studies have focused on the impact of local sea ice loss on Arctic wetting (*2*, *15*), this study further reveals the critical role of AMV phase transitions in regulating Arctic sea ice loss and wetting. This is essential for predicting the spatial variability of near-term future Arctic sea ice loss and wetting, particularly in the North Atlantic sector. As a highly sensitive climate region, the intensified local water cycle in the Atlantic sector of the Arctic not only results in a warmer and wetter atmosphere but also accelerates cryospheric retreat (*50*). This, in turn, enhances freshwater input and ocean stratification in the Atlantic sector and affects soil moisture, runoff variability, and ecosystem stability along the Eurasian Arctic coast (*51*, *52*). These changes disrupt both terrestrial and marine food webs, potentially affecting human activities in the Eurasian Arctic (*51*, *53*, *54*). Therefore, incorporating AMV phase changes into near-term projections of Arctic sea ice loss and wetting is crucial for improving reliability, as existing studies have shown that Arctic sea ice projections are improved when OHT associated with AMV is initialized (*55*, *56*). This will provide a scientific foundation for adaptation strategies in Arctic-bordering countries.

MATERIALS AND METHODS

Observational and reanalysis datasets

Since the Arctic stations were sparse and mostly distributed over Arctic land, we analyzed total precipitation from three reanalysis datasets: ERA5, with a horizontal resolution of about 0.25° by 0.25° (*57*); Japanese 55-year Reanalysis (JRA55), with a horizontal resolution of about 1.25° by 1.25° (*58*); and National Centers for Environmental Prediction-Department of Energy Reanalysis 2 (NCEP2), with a horizontal resolution of 2.5° by 2.5° (*59*). The selected time period is 1979–2024 for ERA5 and NCEP2 and 1979–2023 for JRA55. Given that the representation capabilities of ERA5 and JRA55 for Arctic precipitation are closest to those of station observations (*2*), these two datasets will be used for subsequent moisture budget analysis.

Observational sea ice was collected from the Hadley Centre Sea Ice and Sea Surface Temperature (HadISST) dataset, version 1 (1° by 1° resolution) (*60*), and we also used sea ice data from 1979 to 2017 from Gridded Monthly Sea Ice Extent and Concentration, 1850 Onward, Version 2 (SIBT1850), with a resolution of 2° by 2° (*61*). Given the discrepancies in SST across different datasets (*62*), we use three long-term SST datasets: HadISST data providing SST records from 1870 onward (*60*), the Extended Reconstructed Sea Surface Temperature Version 5 (ERSST V5) produced by National Oceanic and Atmospheric Administration (NOAA), which offers SST data at 2° by 2° latitude-longitude resolution from 1854 to the present (*63*), and the Kaplan Extended SST Version 2 (Kaplan V2) dataset spanning from 1856, derived from comprehensive historical SST observations at 5° by 5° resolution and developed by the Lamont-Doherty Earth Observatory of Columbia University (*64*).

In addition, to investigate atmospheric circulation changes on interdecadal timescales, this study also use SLP, Z500, zonal wind (u), meridional wind (v), and vertical velocity (omega) from two reanalysis datasets: ERA5 covering 1941–2024, and the Twentieth Century Reanalysis Version 3 (NOAA-20CRV3) spanning 1910–2015, which is provided at a horizontal resolution of 1° by 1° (*65*). The zonal velocity (u_o) and potential temperature (θ) of seawater required for calculating oceanic heat transport are derived from the Ocean Reanalysis System 5 (ORAS5), which is produced by the ECMWF operational ensemble reanalysis-analysis system. The ORAS5 dataset spans from 1979 to 2024 with a high spatial resolution of 0.25° by 0.25° (*66*).

Single-model initial-condition large ensembles

To explore the effects of external forcing and internal variability on Arctic wetting, we used SMILE experiments that include a large number of members of a single model, with each member forced by the same historical external forcings but starting from different initial conditions (*37*, *67*). In this study, we mainly used a fully coupled 50-member ensemble from the CESM2 large ensemble simulation, driven by historical forcing from 1850–2014 and SSP3-7.0 forcing thereafter (*68*). These members were driven by smoothed Coupled Model Intercomparison Project phase 6 (CMIP6) biomass burning (BMB) aerosol forcing, which, compared to members driven by the original CMIP6 BMB forcing, provides better comparability with historical observations in terms of Arctic sea ice and temperature simulations (*69*). A previous study on Arctic atmospheric rivers has also used these 50 members (*12*). Monthly total precipitation, evaporation, surface pressure, specific humidity, horizontal wind, vertical velocity, SLP, geopotential height, SIC and SST, zonal velocity, and potential temperature of seawater outputs were used. This study examines the historical period of 1979–2024 and the near-term future period from 2025 to 2054. Since the historical simulations only extend to 2014, the SSP3-7.0 scenario is used to bridge the gap from 2015 to 2024.

To ensure the robustness of the results, we analyzed other seven SMILEs from CMIP6 (*70*): ACCESS-ESM1-5, CanESM5, CNRM-CM6-1, GISS-E2-1-G, IPSL-CM6A-LR, MIROC6, and MPI-ESM1-2-LR, each with over 30 ensemble members to distinguish forced

signals from internal variability (table S1). All models were interpolated onto a common 1° by 1° grid by bilinear interpolation to ensure a consistent basis for comparison and to avoid introducing biases in the analysis arising from different model resolutions. When analyzing the multimodel mean of SMILEs, we first computed the ensemble mean for each model and then performed an equal-weighted multimodel average to avoid bias caused by uneven ensemble sizes. Among these models, ACCESS-ESM1-5, CanESM5, and MPI-ESM1-2-LR provide complete large ensemble members for the future period under SSP1-2.6, SSP2-4.5, and SSP5-8.5 scenarios, with their historical periods extended to 2024 using SSP2-4.5. The remaining models lack large ensemble members for future scenarios, and their historical analysis is limited to 2014. It is worth noting that GISS-E2-1-G does not provide sea ice output.

Moisture budget equation

To explore what controls Arctic wetting and its trend, this study adopts the moisture budget method, which is widely used in various regions (*2*, *71*). The moisture budget equation is represented as follows

$$P = -\partial_t <q> \; - <\nabla \cdot \vec{V} q> + E + \delta \tag{1}$$

where P, E, and q represent total precipitation, evaporation, and specific humidity, respectively. $\vec{V}$ denotes the horizontal wind vector, and δ represents the residual term that accounts for contributions from surface processes due to topography, transient eddies, and the error originating from the representing derivations by finite difference (*72*). $-\partial_t <q>$ denotes the time derivate of the vertically integrated specific humidity, which can generally be ignored, as its annual mean value is significantly smaller than the other terms (*71*). The angle brackets (<>) indicate the vertical integration from the surface to the top of the troposphere (200 hPa)

$$X = \frac{1}{g}\int_{P_S}^{P_T} X dp \tag{2}$$

where g represents the standard gravity, P_S and P_T are surface pressure and the pressure at the top of the troposphere. The term $-<\nabla \cdot \vec{V} q>$ represents the vertically integrated moisture flux convergence and can be further decomposed into a horizontal moisture advection term $-<\overrightarrow{V_h} \cdot \nabla_h q>$ (written as $-<V \cdot \nabla q>$) and a vertical moisture advection term $-<w\frac{\partial q}{\partial p}>$(written as $-<w\,\partial q/\partial p>$). Thus, Eq. 1 can be written as

$$P = -<w\frac{\partial q}{\partial p}> - <\overrightarrow{V_h} \cdot \nabla_h q> + E + \delta \tag{3}$$

where w represents the pressure velocity and $\overrightarrow{V_h}$ represents the horizontal wind vector.

Definition of the OHT through the BSO

We calculated the zonal OHT through BSO at 20°E during 1979–2024 as follows (*73*, *74*)

$$\mathrm{OHT}_{\mathrm{BSO}}(t) = \rho C_p \int_{y1}^{y2}\int_{z}^{0} u_o \theta dz dy \tag{4}$$

where y_1 and y_2 are the latitudes that are chosen (71°N and 73°N), u_o is the zonal velocity of the ocean, and θ is the potential temperature of seawater. ρ is the density of seawater (1027 kg/m^3), C_p is the heat capacity of seawater at constant pressure (3985 J/kg per degree Celsius), and z is the ocean depth that sets to −300 m.

Separating externally forced and internally generated variability

We used SMILEs to separate the impact of external forcing and internal variability (*75*). For example, in CESM2, all 50 members were driven by the same external forcing, with differences arising only from different initial conditions, reflecting internal variability. The effect of internal variability can be partially removed by averaging all members (hereafter "ensemble mean"). Therefore, the ensemble mean of each variable at a certain grid represents the model's response to external forcing (V_{EM}). Then, the internal variability of each variable $V_{IV}(i,t)$ of member i in SMILE

$$V_{IV}(i,t) = V(i,t) - V_{EM}(t) \tag{5}$$

where i refers to the number of members for an SMILE and t refers to the year.

Definition of the AMV and IPO

The observed AMV index is defined as the linearly detrended 11-year moving-average time series of the mean SST anomalies over the North Atlantic (80°W to 0°, 0°N to 60°N). The observed IPO index is calculated as $\mathrm{SST}_2 - (\mathrm{SST}_1 + \mathrm{SST}_3)/2$, where SST_1, SST_2, and SST_3 are defined as the linearly detrended, 11-year moving average time series of the mean SST anomalies over three regions, respectively: the northwestern Pacific (140°E to 145 W°, 25°N to 45°N), equatorial central-eastern Pacific (170°E to 90 W°, 10°S to 10°N), and the southwestern Pacific (150°E to 160 W°, 50°S to 15°S) (*26*). For SMILEs, we subtracted the ensemble mean SST from each member at each grid point in the SMILEs to produce the unforced fields. Then, we computed the mean SST anomalies for the respective regions using the same method as for the observations and derived the AMV and IPO time series.

Evaluation of the AMV and IPO in SMILEs

This study evaluates model performance in simulating temporal variability and spatial patterns of AMV and IPO. We identified three primary metrics: the frequency with which observed values fall above the ensemble maximum, below the ensemble minimum, and within the 90th percentile of the ensemble range (5 to 95%) across all simulated years. If the observed range completely exceeds the ensemble range of a SMILE throughout the entire period, then it can be determined that the deviation between the distribution in that SMILE and observations cannot be explained by internal variability (*76*, *77*). In addition, we characterized the AMV/IPO amplitude in observations and SMILEs using 1 SD of the AMV/IPO index during the entire period. If the observed amplitude range falls within the 25th to 75th percentile of the ensemble range, then the model is considered to be capable of capturing the observed AMV/IPO amplitude (figs. S14 and S15). For spatial patterns, we obtained the observed and simulated AMV/IPO spatial patterns by regressing the AMV/IPO index onto the SST anomalies spatial field and calculated the ensemble mean spatial pattern for each SMILE. If the pattern correlation exceeds 0.5, then the SMILE is considered to adequately represent the observed AMV/IPO pattern (figs. S16 and S17). Among the eight SMILEs used in this study, four models can describe the observed AMV time series, amplitude, and spatial patterns: CESM2, CNRM-CM6-1, IPSL-CM6A-LR, and MPI-ESM1-2-LR.

Three models can represent the observed IPO: CESM2, MIROC6, and MPI-ESM1-2-LR.

AMV-based grouping of ensemble members

We identified members that exhibited pronounced phase transitions in AMV during the period consistent with observations. If AMV transitioned from a negative to a positive phase during 1979–2024, with the index trend being statistically significant at the 95% confidence level based on the Student's *t* test, then the member was classified as having undergone a pronounced negative-to-positive phase transition. Conversely, if the index transitioned from a positive to a negative phase and the index trend is statistically significant at the 95% confidence level based on the Student's *t* test, then it was classified as a pronounced positive-to-negative phase transition. The remaining ensemble members were classified as having no significant phase transition, and the actual SST changes over the North Atlantic region for each group are shown (fig. S9).

The projected uncertainty contributed by the AMV in the near-term future

Following previous studies (*12*, *75*), we conducted the following calculations to determine the impacts of AMV on the projected uncertainty

$$V_{\mathrm{non-AMV}}(i,t) = V_{\mathrm{IV}}(n,i) - r_{\mathrm{IV}}\mathrm{AMV}(i) \times \mathrm{AMV}(i,t) \quad (6)$$

where $r_{\mathrm{IV}}\mathrm{AMV}(i) \times \mathrm{AMV}(i,t)$ refers to the component linearly associated with the AMV index in each member of SMILEs. We estimated the contribution of the AMV to the uncertainty in the projection of Arctic wetting trends by comparing the SD of the trend distribution for all original members $[V_{\mathrm{IV}}(n,i)]$ with the SD of the trend distribution after removing the effects of AMV$\left[V_{\mathrm{non-AMV}}(i,t)\right]$.

Adjustment of Arctic sea ice loss and wetting based on observational AMV

Many studies have applied an "adjustment method" to investigate the climate response to the AMV or IPO (*75*, *76*). Similarly, we performed the adjustment using the AMV. The core idea of this method is to replace the original simulated AMV-related Arctic sea ice loss and wetting with that induced by observed or a hypothetical (observationally based) AMV evolution, expressed as

$$\partial_t V_{\mathrm{adj}}(i) = \partial_t V_{\mathrm{EM}} + \partial_t V_{\mathrm{IV_{adj}}}(i) \quad (7)$$

where

$$\partial_t V_{\mathrm{IV_{adj}}}(i) = \partial_t V_{\mathrm{IV}}(i) + A_{\mathrm{IV}}(i) \quad (8)$$

$A_{\mathrm{IV}}(i)$ is the adjusted term, which can be calculated as follows

$$A_{\mathrm{IV\_AMV}}(i) = -r_{\mathrm{IV}}\mathrm{AMV}(i)\left[\partial_t \mathrm{AMV}(i) - \partial_t \mathrm{AMV}_{\mathrm{OBS}}\right] \quad (9)$$

where $r_{\mathrm{IV}}\mathrm{AMV}(i)$ is the regression coefficient of Arctic sea ice, evaporation, and precipitation on the AMV index during the study period for each member, reflecting the response of Arctic sea ice loss and wetting to AMV evolution in member i. The first product, $r_{\mathrm{IV}}\mathrm{AMV}(i)[\partial_t \mathrm{AMV}(i)]$, denotes the original AMV-related Arctic sea ice loss and wetting trend in member i, while $r_{\mathrm{IV}}\mathrm{AMV}(i)[\partial_t \mathrm{AMV}_{\mathrm{OBS}}]$ denotes the Arctic sea ice loss and wetting trend based on observed AMV evolution. In Eq. 7, $\partial_t V_{\mathrm{EM}}$ refers to the Arctic sea ice loss and wetting response to external forcing, and the ensemble mean of $\partial_t V_{\mathrm{IV_{adj}}}(i)$ represents the trend due to the observed AMV.

Supplementary Materials

This PDF file includes:

Figs. S1 to S17
Table S1

REFERENCES

1. A. Dobler, R. E. Benestad, C. Lussana, O. Landgren, CMIP6 models project a shrinking precipitation area. *NPJ Clim. Atmos. Sci.* **7**, 239 (2024).
2. Z. Cai, Q. You, H. W. Chen, R. Zhang, Z. Zuo, D. Chen, J. Cohen, J. A. Screen, Assessing Arctic wetting: Performances of CMIP6 models and projections of precipitation changes. *Atmos. Res.* **297**, 107124 (2024).
3. R. Bintanja, O. Andry, Towards a rain-dominated Arctic. *Nat. Clim. Chang.* **7**, 263–267 (2017).
4. M. R. McCrystall, J. Stroeve, M. Serreze, B. C. Forbes, J. A. Screen, New climate models reveal faster and larger increases in Arctic precipitation than previously projected. *Nat. Commun.* **12**, 6765 (2021).
5. J. E. Box, W. T. Colgan, T. R. Christensen, N. M. Schmidt, M. Lund, F.-J. W. Parmentier, R. Brown, U. S. Bhatt, E. S. Euskirchen, V. E. Romanovsky, J. E. Walsh, J. E. Overland, M. Wang, R. W. Corell, W. N. Meier, B. Wouters, S. Mernild, J. Mård, J. Pawlak, M. S. Olsen, Key indicators of Arctic climate change: 1971–2017. *Environ. Res. Lett.* **14**, 045010 (2019).
6. T. Dou, C. Xiao, J. Liu, W. Han, Z. Du, A. R. Mahoney, J. Jones, H. Eicken, A key factor initiating surface ablation of Arctic sea ice: Earlier and increasing liquid precipitation. *Cryosphere* **13**, 1233–1246 (2019).
7. J. A. Screen, I. Simmonds, Declining summer snowfall in the Arctic: Causes, impacts and feedbacks. *Climate Dynam.* **38**, 2243–2256 (2012).
8. E. Hanna, D. Topál, J. E. Box, S. Buzzard, F. D. W. Christie, C. Hvidberg, M. Morlighem, L. De Santis, A. Silvano, F. Colleoni, I. Sasgen, A. F. Banwell, M. R. van den Broeke, R. DeConto, J. De Rydt, H. Goelzer, A. Gossart, G. H. Gudmundsson, K. Lindbäck, B. Miles, R. Mottram, F. Pattyn, R. Reese, E. Rignot, A. Srivastava, S. Sun, J. Toller, P. A. Tuckett, L. Ultee, Short- and long-term variability of the Antarctic and Greenland Ice Sheets. *Nat. Rev. Earth Environ.* **5**, 193–210 (2024).
9. B. C. Forbes, T. Kumpula, N. Meschtyb, R. Laptander, M. Macias-Fauria, P. Zetterberg, M. Verdonen, A. Skarin, K.-Y. Kim, L. N. Boisvert, J. C. Stroeve, A. Bartsch, Sea ice, rain-on-snow and tundra reindeer nomadism in Arctic Russia. *Biol. Lett.* **12**, 20160466 (2016).
10. E. Post, R. B. Alley, T. R. Christensen, M. Macias-Fauria, B. C. Forbes, M. N. Gooseff, A. Iler, J. T. Kerby, K. L. Laidre, M. E. Mann, J. Olofsson, J. C. Stroeve, F. Ulmer, R. A. Virginia, M. Y. Wang, The polar regions in a 2°C warmer world. *Sci. Adv.* **5**, eaaw9883 (2019).
11. D. White, L. Hinzman, L. Alessa, J. Cassano, M. Chambers, K. Falkner, J. Francis, W. J. Gutowski Jr., M. Holland, R. M. Holmes, H. Huntington, D. Kane, A. Kliskey, C. Lee, J. McClelland, B. Peterson, T. S. Rupp, F. Straneo, M. Steele, R. Woodgate, D. Yang, K. Yoshikawa, T. Zhang, The arctic freshwater system: Changes and impacts. *J. Geophys. Res. Biogeo.* **112**, G04S54 (2007).
12. W. Ma, H. Wang, G. Chen, L. R. Leung, J. Lu, P. J. Rasch, Q. Fu, B. Kravitz, Y. Zou, J. J. Cassano, W. Maslowski, The role of interdecadal climate oscillations in driving Arctic atmospheric river trends. *Nat. Commun.* **15**, 2135 (2024).
13. A. Dufour, O. Zolina, S. K. Gulev, Atmospheric moisture transport to the Arctic: Assessment of reanalyses and analysis of transport components. *J. Climate* **29**, 5061–5081 (2016).
14. R. Bintanja, K. van der Wiel, E. C. van der Linden, J. Reusen, L. Bogerd, F. Krikken, F. M. Selten, Strong future increases in Arctic precipitation variability linked to poleward moisture transport. *Sci. Adv.* **6**, eaax6869 (2020).
15. R. Bintanja, F. M. Selten, Future increases in Arctic precipitation linked to local evaporation and sea-ice retreat. *Nature* **509**, 479–482 (2014).
16. Q. Zhang, B. Huai, M. Ding, W. Sun, W. Liu, J. Yan, S. Zhao, Y. Wang, Y. Wang, L. Wang, J. Che, J. Dou, L. Kang, Projections of Greenland climate change from CMIP5 and CMIP6. *Global Planet. Change* **232**, 104340 (2024).
17. Z. Cai, Q. You, J. A. Screen, H. W. Chen, R. Zhang, Z. Zuo, D. Chen, J. Cohen, S. Kang, R. Zhang, Lessened projections of Arctic warming and wetting after correcting for model errors in global warming and sea ice cover. *Sci. Adv.* **11**, eadr6413 (2025).
18. D. Notz, How well must climate models agree with observations? *Philos. Trans. A Math. Phys. Eng. Sci.* **373**, 20140164 (2015).
19. Z. Li, T. Liu, Y. Huang, J. Peng, Y. Ling, Evaluation of the CMIP6 precipitation simulations over global land. *Earth's Future* **10**, e2021EF002500 (2022).
20. A. J. Sweeney, Q. Fu, S. Po-Chedley, H. Wang, M. Wang, Internal variability increased Arctic amplification during 1980–2022. *Geophys. Res. Lett.* **50**, e2023GL106060 (2023).
21. N. C. Swart, J. C. Fyfe, E. Hawkins, J. E. Kay, A. Jahn, Influence of internal variability on Arctic sea-ice trends. *Nat. Clim. Chang.* **5**, 86–89 (2015).
22. R. Zhang, Mechanisms for low-frequency variability of summer Arctic sea ice extent. *Proc. Natl. Acad. Sci. U.S.A.* **112**, 4570–4575 (2015).
23. Q. Ding, A. Schweiger, M. L'Heureux, E. J. Steig, D. S. Battisti, N. C. Johnson, E. Blanchard-Wrigglesworth, S. Po-Chedley, Q. Zhang, K. Harnos, M. Bushuk, B. Markle,

I. Baxter, Fingerprints of internal drivers of Arctic sea ice loss in observations and model simulations. *Nat. Geosci.* **12**, 28–33 (2019).
24. D. Li, R. Zhang, T. R. Knutson, On the discrepancy between observed and CMIP5 multi-model simulated Barents Sea winter sea ice decline. *Nat. Commun.* **8**, 14991 (2017).
25. W. Zhou, L. R. Leung, J. Lu, Steady threefold Arctic amplification of externally forced warming masked by natural variability. *Nat. Geosci.* **17**, 508–515 (2024).
26. X. Chen, A. Dai, Quantifying contributions of external forcing and internal variability to Arctic warming during 1900–2021. *Earth's Future* **12**, e2023EF003734 (2024).
27. D. D. Bokuchava, V. A. Semenov, Mechanisms of the early 20th century warming in the Arctic. *Earth Sci. Rev.* **222**, 103820 (2021).
28. M. Fang, X. Li, H. W. Chen, D. Chen, Arctic amplification modulated by Atlantic multidecadal oscillation and greenhouse forcing on multidecadal to century scales. *Nat. Commun.* **13**, 1865 (2022).
29. P. Chylek, C. K. Folland, G. Lesins, M. K. Dubey, M. Wang, Arctic air temperature change amplification and the Atlantic multidecadal oscillation. *Geophys. Res. Lett.* **36**, L14801 (2009).
30. F. S. Castruccio, Y. Ruprich-Robert, S. G. Yeager, G. Danabasoglu, R. Msadek, T. L. Delworth, Modulation of Arctic sea ice loss by atmospheric teleconnections from Atlantic Multidecadal Variability. *J. Climate* **32**, 1419–1441 (2019).
31. Z. He, A. Dai, B. E. J. Rose, M. Vuille, Influence of the Atlantic and Pacific multidecadal variability on Arctic sea ice in pacemaker simulations during 1920–2013. *J. Climate* **37**, 4481–4506 (2024).
32. Y. Ruprich-Robert, R. Msadek, F. Castruccio, S. Yeager, T. Delworth, G. Danabasoglu, Assessing the climate impacts of the observed Atlantic Multidecadal Variability using the GFDL CM2.1 and NCAR CESM1 global coupled models. *J. Climate* **30**, 2785–2810 (2017).
33. G. A. Meehl, A. Hu, F. Castruccio, M. H. England, S. C. Bates, G. Danabasoglu, S. McGregor, J. M. Arblaster, S.-P. Xie, N. Rosenbloom, Atlantic and Pacific tropics connected by mutually interactive decadal-timescale processes. *Nat. Geosci.* **14**, 36–42 (2021).
34. K. Schwarzwald, N. Lenssen, The importance of internal climate variability in climate impact projections. *Proc. Natl. Acad. Sci. U.S.A.* **119**, e2208095119 (2022).
35. X. Huang, T. Zhou, A. Dai, H. Li, C. Li, X. Chen, J. Lu, J.-S. Von Storch, B. Wu, South Asian summer monsoon projections constrained by the Interdecadal Pacific Oscillation. *Sci. Adv.* **6**, eaay6546 (2020).
36. M. Rantanen, Natural variability boosts Arctic warming. *Nat. Geosci.* **17**, 485–486 (2024).
37. C. Deser, F. Lehner, K. B. Rodgers, T. Ault, T. L. Delworth, P. N. DiNezio, A. Fiore, C. Frankignoul, J. C. Fyfe, D. E. Horton, J. E. Kay, R. Knutti, N. S. Lovenduski, J. Marotzke, K. A. McKinnon, S. Minobe, J. Randerson, J. A. Screen, I. R. Simpson, M. Ting, Insights from Earth system model initial-condition large ensembles and future prospects. *Nat. Clim. Chang.* **10**, 277–286 (2020).
38. K. B. Tokarska, M. B. Stolpe, S. Sippel, E. M. Fischer, C. J. Smith, F. Lehner, R. Knutti, Past warming trend constrains future warming in CMIP6 models. *Sci. Adv.* **6**, eaaz9549 (2020).
39. C. X. Wang, R. M. Graham, K. G. Wang, S. Gerland, M. A. Granskog, Comparison of ERA5 and ERA-Interim near-surface air temperature, snowfall and precipitation over Arctic sea ice: Effects on sea ice thermodynamics and evolution. *Cryosphere* **13**, 1661–1679 (2019).
40. Q. Ding, J. M. Wallace, D. S. Battisti, E. J. Steig, A. J. E. Gallant, H.-J. Kim, L. Geng, Tropical forcing of the recent rapid Arctic warming in northeastern Canada and Greenland. *Nature* **509**, 209–212 (2014).
41. J. A. Screen, C. Deser, Pacific Ocean Variability influences the time of emergence of a seasonally ice-free Arctic Ocean. *Geophys. Res. Lett.* **46**, 2222–2231 (2019).
42. J. T. Fasullo, A. S. Phillips, C. Deser, Evaluation of leading modes of climate variability in the CMIP archives. *J. Climate* **33**, 5527–5545 (2020).
43. Z. Liu, C. Risi, F. Codron, X. He, C. J. Poulsen, Z. Wei, D. Chen, S. Li, G. J. Bowen, Acceleration of western Arctic sea ice loss linked to the Pacific North American pattern. *Nat. Commun.* **12**, 1519 (2021).
44. R. Hand, J. Bader, D. Matei, R. Ghosh, J. H. Jungclaus, Changes of decadal SST variations in the subpolar north Atlantic under strong CO_2 forcing as an indicator for the ocean circulation's contribution to Atlantic Multidecadal Variability. *J. Climate* **33**, 3213–3228 (2020).
45. S. Li, L. Wu, Y. Wang, T. Geng, W. Cai, B. Gan, Z. Jing, Y. Yang, Intensified Atlantic Multidecadal Variability in a warming climate. *Nat. Clim. Chang.* **15**, 293–300 (2025).
46. Y. Peings, G. Magnusdottir, Wintertime atmospheric response to Atlantic Multidecadal Variability: Effect of stratospheric representation and ocean–atmosphere coupling. *Climate Dynam.* **47**, 1029–1047 (2016).
47. Y. Okumura, S.-P. Xie, A. Numaguti, Y. Tanimoto, Tropical Atlantic air-sea interaction and its influence on the NAO. *Geophys. Res. Lett.* **28**, 1507–1510 (2001).
48. C. Wang, H. Su, C. Zhai, J. Zheng, S. Yu, H. Mo, Y. Wang, L. Jiang, Recent slowing of Arctic sea ice melt tied to multidecadal NAO variability. *Nat. Commun.* **16**, 8504 (2025).
49. Z. Liu, Z. Li, W. Xu, X. Huan, H. Lan, Recent intensification of Arctic winter anticyclonic circulation linked to local sea ice loss and SST warming. *J. Geophys. Res. Atmos.* **130**, e2025JD044995 (2025).
50. T. Vihma, Effects of Arctic sea ice decline on weather and climate: A review. *Surv. Geophys.* **35**, 1175–1214 (2014).
51. R. Gou, K. K. E. Wolf, C. J. M. Hoppe, L. Wu, G. Lohmann, The changing nature of future Arctic marine heatwaves and its potential impacts on the ecosystem. *Nat. Clim. Chang.* **15**, 162–170 (2025).
52. A. Bring, I. Fedorova, Y. Dibike, L. Hinzman, J. Mård, S. H. Mernild, T. Prowse, O. Semenova, S. L. Stuefer, M.-K. Woo, Arctic terrestrial hydrology: A synthesis of processes, regional effects, and research challenges. *J. Geophys. Res. Biogeo.* **121**, 621–649 (2016).
53. T. Vihma, J. Screen, M. Tjernström, B. Newton, X. Zhang, V. Popova, C. Deser, M. Holland, T. Prowse, The atmospheric role in the Arctic water cycle: A review on processes, past and future changes, and their impacts. *J. Geophys. Res. Biogeo.* **121**, 586–620 (2016).
54. A. Instanes, V. Kokorev, R. Janowicz, O. Bruland, K. Sand, T. Prowse, Changes to freshwater systems affecting Arctic infrastructure and natural resources. *J. Geophys. Res. Biogeo.* **121**, 567–585 (2016).
55. S. G. Yeager, A. R. Karspeck, G. Danabasoglu, Predicted slowdown in the rate of Atlantic sea ice loss. *Geophys. Res. Lett.* **42**, 10704–10713 (2015).
56. S. Yeager, A. Karspeck, G. Danabasoglu, J. Tribbia, H. Teng, A decadal prediction case study: Late twentieth-century north Atlantic ocean heat content. *J. Climate* **25**, 5173–5189 (2012).
57. H. Hersbach, B. Bell, P. Berrisford, S. Hirahara, A. Horanyi, J. Munoz-Sabater, J. Nicolas, C. Peubey, R. Radu, D. Schepers, A. Simmons, C. Soci, S. Abdalla, X. Abellan, G. Balsamo, P. Bechtold, G. Biavati, J. Bidlot, M. Bonavita, G. De Chiara, P. Dahlgren, D. Dee, M. Diamantakis, R. Dragani, J. Flemming, R. Forbes, M. Fuentes, A. Geer, L. Haimberger, S. Healy, R. J. Hogan, E. Holm, M. Janiskova, S. Keeley, P. Laloyaux, P. Lopez, C. Lupu, G. Radnoti, P. de Rosnay, I. Rozum, F. Vamborg, S. Villaume, J. N. Thepaut, The ERA5 global reanalysis. *Q. J. Roy. Meteorol. Soc.* **146**, 1999–2049 (2020).
58. A. Ebita, S. Kobayashi, Y. Ota, M. Moriya, R. Kumabe, K. Onogi, Y. Harada, S. Yasui, K. Miyaoka, K. Takahashi, H. Kamahori, C. Kobayashi, H. Endo, M. Soma, Y. Oikawa, T. Ishimizu, The Japanese 55-year reanalysis "JRA-55": An interim report. *SOLA* **7**, 149–152 (2011).
59. M. Kanamitsu, W. Ebisuzaki, J. Woollen, S.-K. Yang, J. J. Hnilo, M. Fiorino, G. L. Potter, NCEP–DOE AMIP-II Reanalysis (R-2). *Bull. Am. Meteorol. Soc.* **83**, 1631–1644 (2002).
60. N. A. Rayner, D. E. Parker, E. B. Horton, C. K. Folland, L. V. Alexander, D. P. Rowell, E. C. Kent, A. Kaplan, Global analyses of sea surface temperature, sea ice, and night marine air temperature since the late nineteenth century. *J. Geophys. Res. Atmos.* **108**, 4407 (2003).
61. J. E. Walsh, F. Fetterer, J. Scott Stewart, W. L. Chapman, A database for depicting Arctic sea ice variations back to 1850. *Geogr. Rev.* **107**, 89–107 (2017).
62. S. Menemenlis, G. A. Vecchi, W. Yang, S. Fueglistaler, S. P. Raghuraman, Consequential differences in satellite-era sea surface temperature trends across datasets. *Nat. Clim. Chang.* **15**, 897–903 (2025).
63. B. Huang, P. W. Thorne, V. F. Banzon, T. Boyer, G. Chepurin, J. H. Lawrimore, M. J. Menne, T. M. Smith, R. S. Vose, H.-M. Zhang, Extended reconstructed sea surface temperature, version 5 (ERSSTv5): Upgrades, validations, and intercomparisons. *J. Climate* **30**, 8179–8205 (2017).
64. A. Kaplan, M. A. Cane, Y. Kushnir, A. C. Clement, M. B. Blumenthal, B. Rajagopalan, Analyses of global sea surface temperature 1856–1991. *J. Geophys. Res.* **103**, 18567–18589 (1998).
65. L. C. Slivinski, G. P. Compo, P. D. Sardeshmukh, J. S. Whitaker, C. McColl, R. J. Allan, P. Brohan, X. Yin, C. A. Smith, L. J. Spencer, R. S. Vose, M. Rohrer, R. P. Conroy, D. C. Schuster, J. J. Kennedy, L. Ashcroft, S. Brönnimann, M. Brunet, D. Camuffo, R. Cornes, T. A. Cram, F. Domínguez-Castro, J. E. Freeman, J. Gergis, E. Hawkins, P. D. Jones, H. Kubota, T. C. Lee, A. M. Lorrey, J. Luterbacher, C. J. Mock, R. K. Przybylak, C. Pudmenzky, V. C. Slonosky, B. Tinz, B. Trewin, X. L. Wang, C. Wilkinson, K. Wood, P. Wyszyński, An evaluation of the performance of the Twentieth Century Reanalysis Version 3. *J. Climate* **34**, 1417–1438 (2021).
66. H. Zuo, M. A. Balmaseda, S. Tietsche, K. Mogensen, M. Mayer, The ECMWF operational ensemble reanalysis–analysis system for ocean and sea ice: A description of the system and assessment. *Ocean Sci.* **15**, 779–808 (2019).
67. C. Deser, A. Phillips, V. Bourdette, H. Teng, Uncertainty in climate change projections: The role of internal variability. *Climate Dynam.* **38**, 527–546 (2012).
68. K. B. Rodgers, S. S. Lee, N. Rosenbloom, A. Timmermann, G. Danabasoglu, C. Deser, J. Edwards, J. E. Kim, I. R. Simpson, K. Stein, M. F. Stuecker, R. Yamaguchi, T. Bódai, E. S. Chung, L. Huang, W. M. Kim, J. F. Lamarque, D. L. Lombardozzi, W. R. Wieder, S. G. Yeager, Ubiquity of human-induced changes in climate variability. *Earth Syst. Dynam.* **12**, 1393–1411 (2021).
69. P. DeRepentigny, A. Jahn, M. M. Holland, J. E. Kay, J. Fasullo, J.-F. Lamarque, S. Tilmes, C. Hannay, M. J. Mills, D. A. Bailey, A. P. Barrett, Enhanced simulated early 21st century Arctic sea ice loss due to CMIP6 biomass burning emissions. *Sci. Adv.* **8**, eabo2405 (2022).
70. V. Eyring, S. Bony, G. A. Meehl, C. A. Senior, B. Stevens, R. J. Stouffer, K. E. Taylor, Overview of the Coupled Model Intercomparison Project Phase 6 (CMIP6) experimental design and organization. *Geosci. Model Dev.* **9**, 1937–1958 (2016).
71. A. A. Akinsanola, W. Zhou, Dynamic and thermodynamic factors controlling increasing summer monsoon rainfall over the West African Sahel. *Climate Dynam.* **52**, 4501–4514 (2019).
72. R. Seager, N. Naik, G. A. Vecchi, Thermodynamic and dynamic mechanisms for large-scale changes in the hydrological cycle in response to global warming. *J. Climate* **23**, 4651–4668 (2010).

73. D. Oldenburg, K. C. Armour, L. Thompson, C. M. Bitz, Distinct mechanisms of ocean heat transport into the Arctic under internal variability and climate change. *Geophys. Res. Lett.* **45**, 7692–7700 (2018).
74. J. Shi, B. Luo, D. Luo, Y. Yao, T. Gong, Y. Liu, Differing roles of North Atlantic oceanic and atmospheric transports in the winter Eurasian Arctic sea-ice interannual-to-decadal variability. *NPJ Clim. Atmos. Sci.* **7**, 62 (2024).
75. J. Jiang, T. Zhou, Agricultural drought over water-scarce Central Asia aggravated by internal climate variability. *Nat. Geosci.* **16**, 154–161 (2023).
76. K. Zhang, Z. Zuo, L. Suarez-Gutierrez, L. Bu, The significant influence of the Atlantic Multidecadal Variability to the abrupt warming in Northeast Asia in the 1990s. *NPJ Clim. Atmos. Sci.* **7**, 28 (2024).
77. L. Suarez-Gutierrez, S. Milinski, N. Maher, Exploiting large ensembles for a better yet simpler climate model evaluation. *Climate Dynam.* **57**, 2557–2580 (2021).

Acknowledgments: We appreciate the comments and suggestions provided by the editors and reviewers. We also thank Fudan University and the University of Exeter for providing the computing platforms. **Funding:** Q.Y. was supported by the National Key Research and Development Program of China under award nos. 2023YFE0123800 and 2022YFF0801703, the Shanghai B&R Joint Laboratory Project by grant no. 22230750300, and the Shanghai Pilot Program for Basic Research–Fudan University by grant no. 22TQ007. Z.C. was supported by the Postdoctoral Fellowship Program of CPSF by grant no. GZB20250074. S.K.G. was supported by RSF grant by grant no. 23-77-30001. J.A.S. was supported by the NERC ArctiCONNECT project by grant no. NE/V005855/1. **Author contributions:** Supervision: Q.Y., S.K., J.A.S., D.C., and R.Z. Methodology: Q.Y. and J.C. Conceptualization: Q.Y., J.C., R.Z., and D.C. Visualization: Z.C., Q.Y., and J.C. Writing—original draft: Z.C., Q.Y., J.A.S., J.C., and G.W.K.M. Writing—review and editing: Q.Y., S.K., J.A.S., H.W.C., R.Z., Z.Z., D.C., J.C., W.M., S.K.G., G.W.K.M., and R.Z. Investigation: Z.C., Q.Y., J.C., and R.Z. Validation: Z.C., Q.Y., J.C., and R.Z. Formal analysis: Z.C., Q.Y., and J.C. Resources: Q.Y. and J.A.S. Funding acquisition: Q.Y. and D.C. Data curation: Q.Y. and R.Z. Software: Q.Y. Project administration: Q.Y. **Competing interests:** The authors declare that they have no competing interests. **Data, code, and materials availability:** All data and code needed to evaluate and reproduce the results in the paper are present in the paper and/or the Supplementary Materials. Additional data are available from the following sources: The SMILEs of CMIP6 outputs are available at https://aims2.llnl.gov/search/cmip6/. The CESM2 outputs are available at www.cesm.ucar.edu/community-projects/lens2. ERA5 is available at https://cds.climate.copernicus.eu/cdsapp#!/dataset/reanalysis-era5-single-levels-monthly-means?tab=overview. JRA55 is available at reanalysis: https://rda.ucar.edu. NCEP2 is available at https://rda.ucar.edu. 20CRV3 is available at https://psl.noaa.gov/data/gridded/data.20thC_ReanV3.html. HadISST dataset is available at www.metoffice.gov.uk/hadobs/hadisst/. SIBT1850 sea ice dataset is available at https://nsidc.org/data/g10010/versions/2. ORAS5 is available at https://cds.climate.copernicus.eu/datasets/reanalysis-oras5?tab=overview. ERSST V5 is available at https://psl.noaa.gov/data/gridded/data.noaa.ersst.v5.html. Kaplan V2 is available at https://psl.noaa.gov/data/gridded/data.kaplan_sst.html. This study did not generate any new materials.

Submitted 5 May 2025
Accepted 26 February 2026
Published 25 March 2026
10.1126/sciadv.ady7595

ScienceAdvances

Role of Atlantic multidecadal variability in modulating Arctic sea ice loss and wetting

Ziyi Cai, Qinglong You, James A. Screen, Hans W. Chen, Ruonan Zhang, Zhiyan Zuo, Deliang Chen, Judah Cohen, Shichang Kang, Weiming Ma, Sergey K. Gulev, G. W. K. Moore, and Renhe Zhang

Sci. Adv. **12** (13), eady7595. DOI: 10.1126/sciadv.ady7595

Science Advances (ISSN 2375-2548) is published by the American Association for the Advancement of Science. 1200 New York Avenue NW, Washington, DC 20005. The title *Science Advances* is a registered trademark of AAAS.